Supporting Information

Green Transformation of Fish-Oil By-Products into Polysulfide-based Nanocomposite Adsorbents via Coupled Inverse Vulcanization and Exfoliation

Mohamed Boundor,[a] Nadia Katir,[a] and Abdelkrim El Kadib.[a,b,*]

[a] Euromed University of Fes, UEMF, Morocco.

[b] Hassan II Academy of Science and Technology, Rabat, Morocco.

Corresponding Author Prof. Dr. Abdelkrim El Kadib, a.elkadib@ueuromed.org

General

Crude fish oil was obtained from the industrial processing of small pelagic fish into fishmeal from Morocco. The raw oil was filtered to remove residual solid particles prior to use. Commercial vegetable oil, consisting predominantly of soybean oil, was used as received. Elemental sulfur (CAS Number: 7704-34-9) was purchased from Sigma-Aldrich and used without further purification. Natural montmorillonite clay (MMT) was obtained from Southern Clay Products Inc. (Gonzales, TX, USA) under the trade name Cloisite-Na^+. Graphene oxide (GO) was synthesized from graphite powder using a modified Hummers' method.[1]

Fourier transform infrared (FT-IR) spectra were obtained with a Perkin-Elmer Spectrum 100FT-IR spectrometer on pure samples (ATR FTIR) at room temperature (25°C). Spectra were collected in 32 scans with a 4 cm^{-1} spectral resolution from 4000 to 399 cm^{-1}. ^1H and ^{13}C liquid NMR spectra were obtained at 25°C on a JEOL 600MHz spectrometer. The chemical shifts (δ) are reported in ppm relative to $Si(CH_3)_4$ for the ^1H and ^{13}C nuclei after calibration of the spectra using the residual solvent of the deuterated chloroform ($CDCl_3$) as an internal reference. The material was first solidified using liquid nitrogen and then ground into a fine powder. This powder was subsequently added to a deuterated solvent in an NMR tube and subjected to prolonged sonication until a visually homogeneous dispersion was obtained. The CHNS/O elemental analyzes were carried out using a Perkin Elmer 2400 series II analyzer. Thermogravimetric analysis (TGA) was carried out with a Mettler Toledo TGA/DSC 3+ thermal analyzer over the range of 25 to 750 °C under air or nitrogen flow (80 mL min^{-1}), at a heating rate of 2 °C min^{-1}. Differential scanning calorimetry (DSC) measurements were performed on a TA Instruments Q100 calorimeter over a temperature range of −20 to 140 °C, using heating and cooling rates of 5 °C min^{-1} under a continuous nitrogen flow of 50 mL min^{-1}. X-ray powder diffraction (XRD) patterns were collected on a Bruker D8 Advanced AXS diffractometer equipped with a monochromatic Cu Kα1 radiation source (λ = 1.5418 Å) and operated at 40 kV and 30 mA. X-ray patterns were recorded in the region of 5–80° with a step size of 0.02° (step time = 0.5 s). Nitrogen sorption isotherms at 77 K were measured with a Micromeritics Tristar II Plus apparatus. Before measurement, samples were degassed for 8 h at 100°C to remove any physisorbed species. The surface area (S_{BET}) was determined by applying the multipoint B.E.T. algorithm on a linear portion at relative pressures between 0.04 and 0.25. The pore volumes were estimated from the volume of nitrogen adsorbed at relative pressure of 0.99. Scanning electron microscopy (SEM) images were taken using a JEOL JSM 6700F equipped with an energy-dispersive X-ray spectroscopy (EDS) detector. The solids were directly deposited on a carbon tape. UV−visible spectroscopy was measured in the 200−800 nm wavelength range on a PerkinElmer Lambda 1050 spectrometer equipped with an integrating sphere.

Metal ions, methylene blue and I2 adsorption

Adsorption experiments were carried out to evaluate the performance of the FO@S-based adsorbents toward Au^{3+}, Fe^{3+}, methylene blue (MB), and iodine (I_2). For each test, a fixed amount of adsorbent (10 mg) was added to 20 mL of the corresponding contaminant solution and the mixture was stirred at room temperature under batch conditions.

For Au^{3+} adsorption, a $HAuCl_4$ aqueous solution with an initial concentration of 307 mg/L was prepared. A volume of 20 mL of this solution was contacted with 10 mg of the adsorbent and the suspension was stirred for 24 h. The remaining concentration of Au^{3+} was quantified using UV–visible spectroscopy at 307 nm. The adsorption of Fe^{3+} was performed similarly using a $FeCl_3$ solution at an initial concentration of 50 mg/L. In this case, 20 mL of the prepared solution was mixed with 10 mg of adsorbent and stirred for 24 h, and the Fe^{3+} concentration after treatment was determined by UV–visible analysis at 300 nm.

Methylene blue adsorption studies were carried out using its solutions at initial concentrations of 160 mg/L or 320 mg/L. In each experiment, 10 mg of adsorbent was added to 20 mL of the dye solution and stirred for 24 h. The residual MB concentration was measured by UV–visible spectroscopy at 657 nm. Iodine adsorption was performed using a hexane solution of I_2 with an initial concentration of 253.8 mg/L. A 20 mL aliquot of this solution was mixed with 10 mg of adsorbent and stirred for 4 h, and the remaining I_2 concentration was monitored at 522 nm.

After adsorption, the FO@S-based materials were separated from the solutions using a strainer, while elemental sulfur (S_8) was removed by centrifugation.

The removal (R, %) and adsorption capacity (Q, mg/g) were calculated using equations (1) and (2). In these equations, C_i is the initial concentration of the solution (mg/L), C_f is the final concentration (mg/L), m is the mass of adsorbent (g), and V is the volume of solution (L):

$$R\ (\%) = (C_i - C_f)*100/C_i \qquad (1)$$

$$Q\ (mg/g) = (C_i - C_f)*V/m \qquad (2)$$

Adsorption isotherm experiments were performed by contacting 10 mg of **FO@S_50:50** with 20 mL of Fe^{3+} solutions at different initial concentrations (10, 25, 50, 100, 150, and 170 mg/L) under continuous agitation for 24 h. After reaching adsorption equilibrium, the suspensions were separated, and the residual Fe^{3+} concentration in the supernatant was determined by UV-vis spectroscopy. The equilibrium adsorption capacity (Q_e, mg/g) was calculated using Equation (2), and adsorption isotherms were obtained by plotting Q_e as a function of the equilibrium concentration (C_e, mg/L).

Figure S1. Visual appearance of fish oil and vegetable oil monomers and their corresponding products obtained via inverse vulcanization.

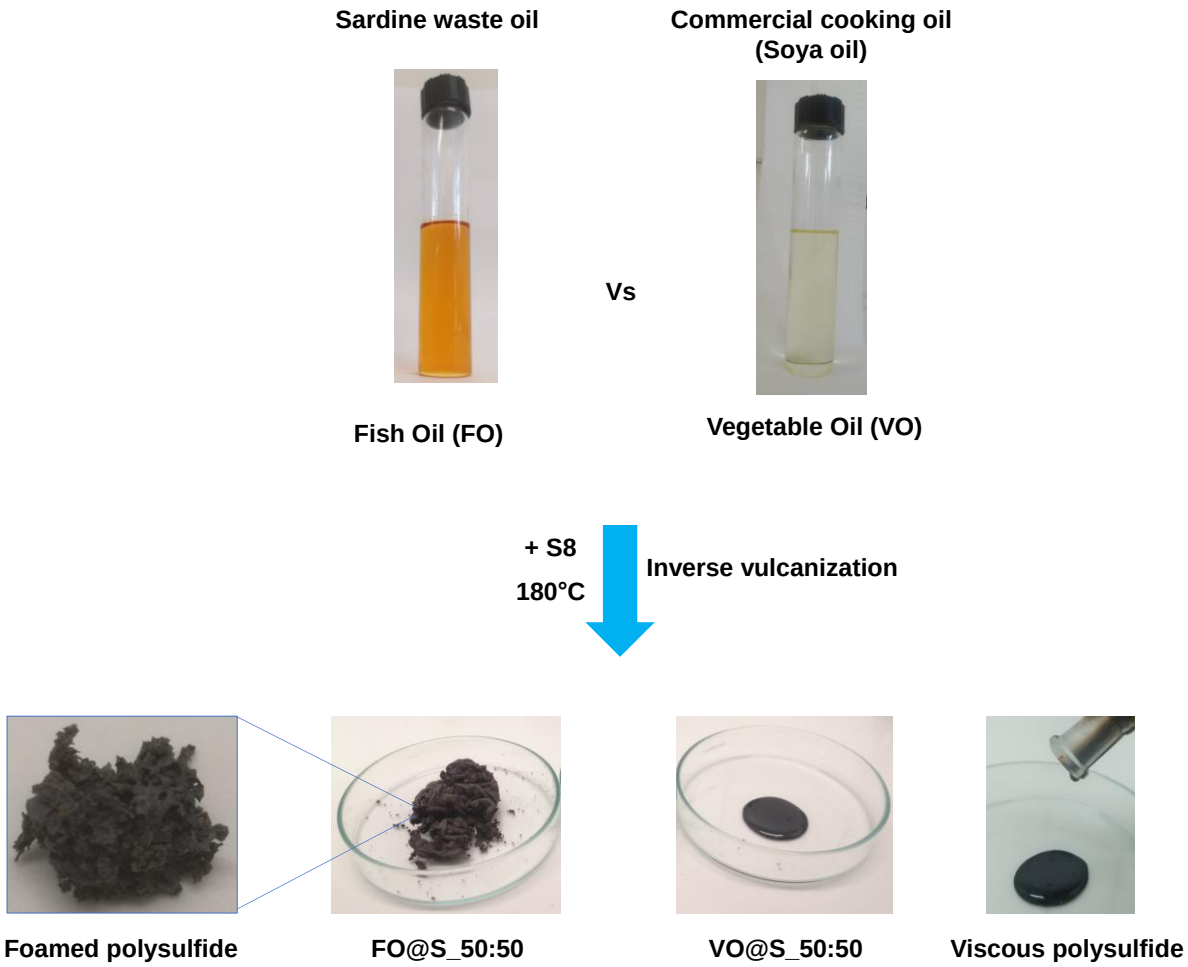

Figure S2. FTIR spectra of **FO** and **FO@S_X:Y**.

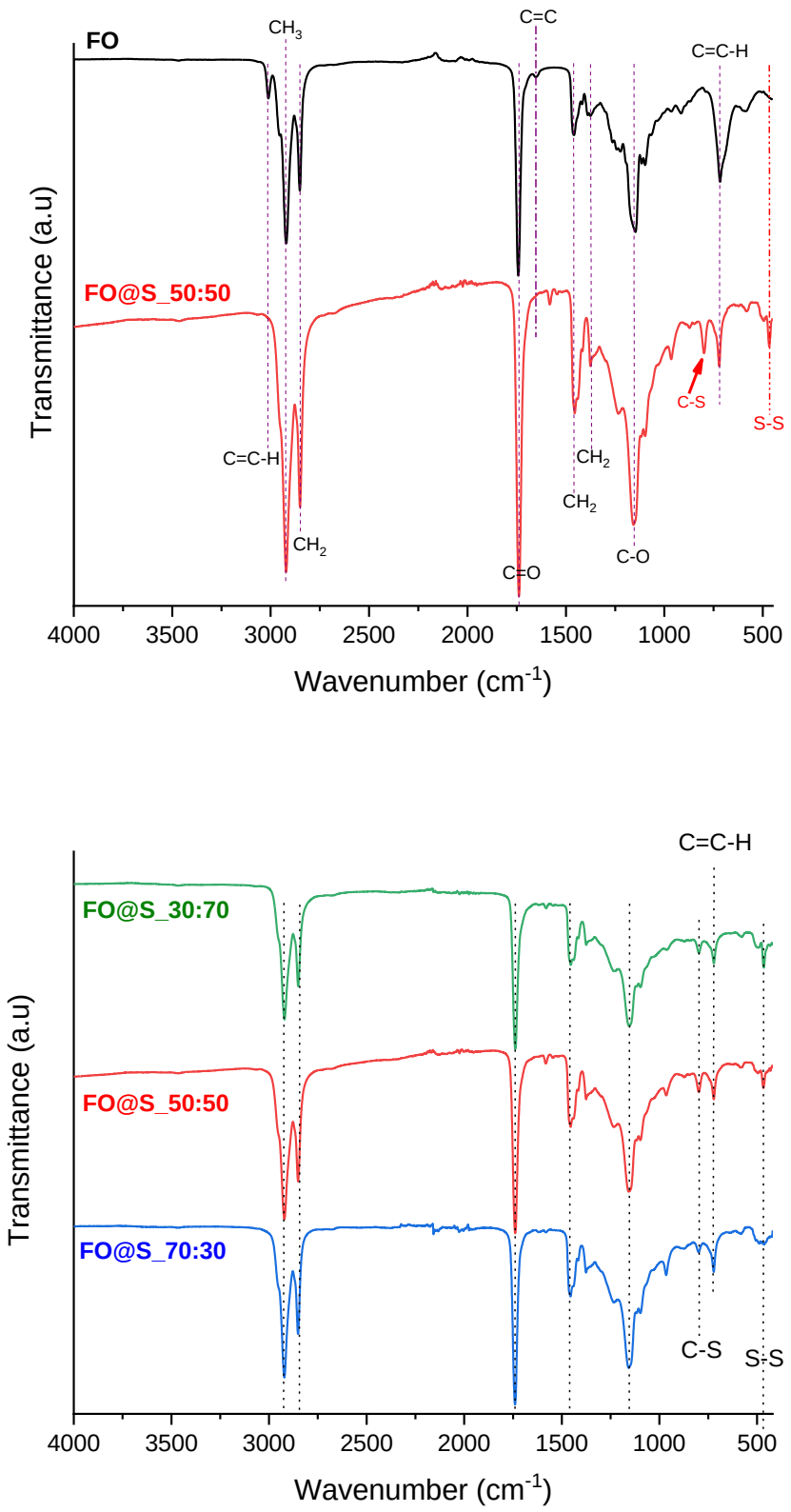

Figure S3. ^{1}H and ^{13}C NMR spectra of **FO** and **FO@S_X:Y**

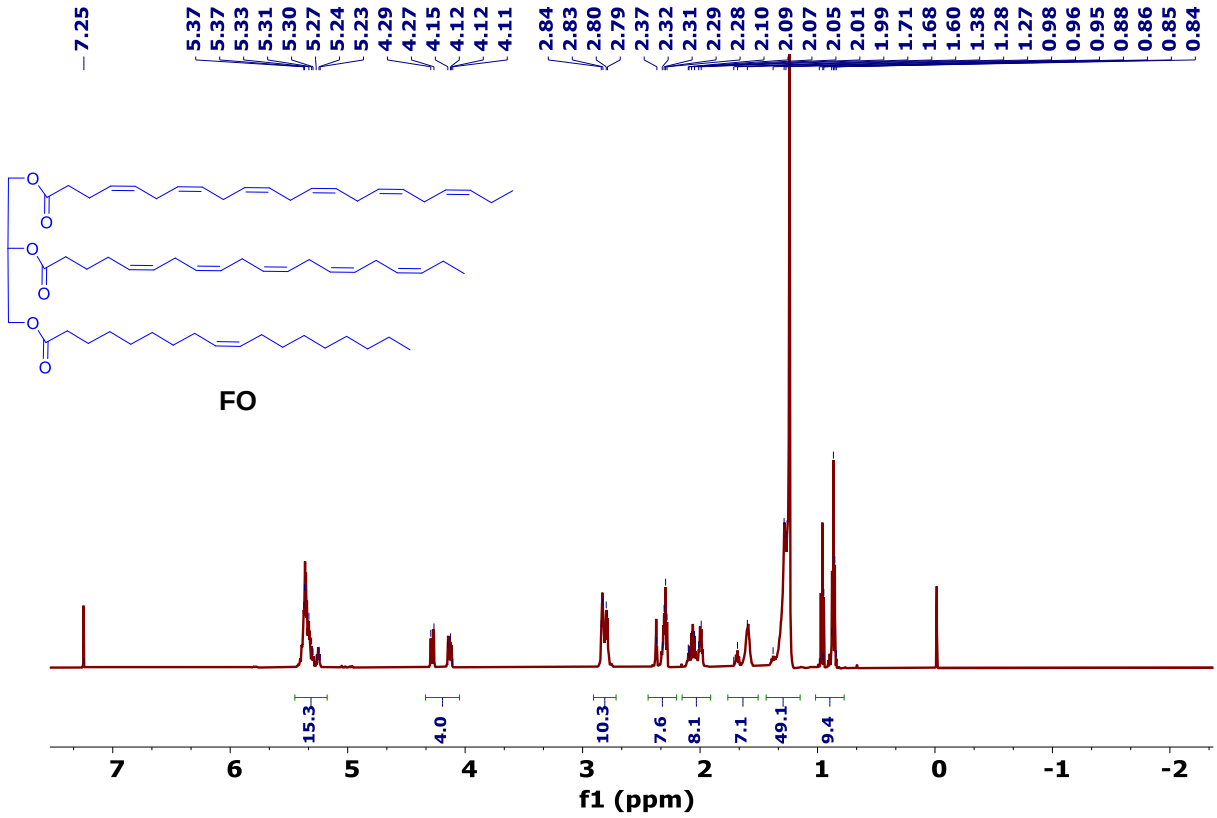

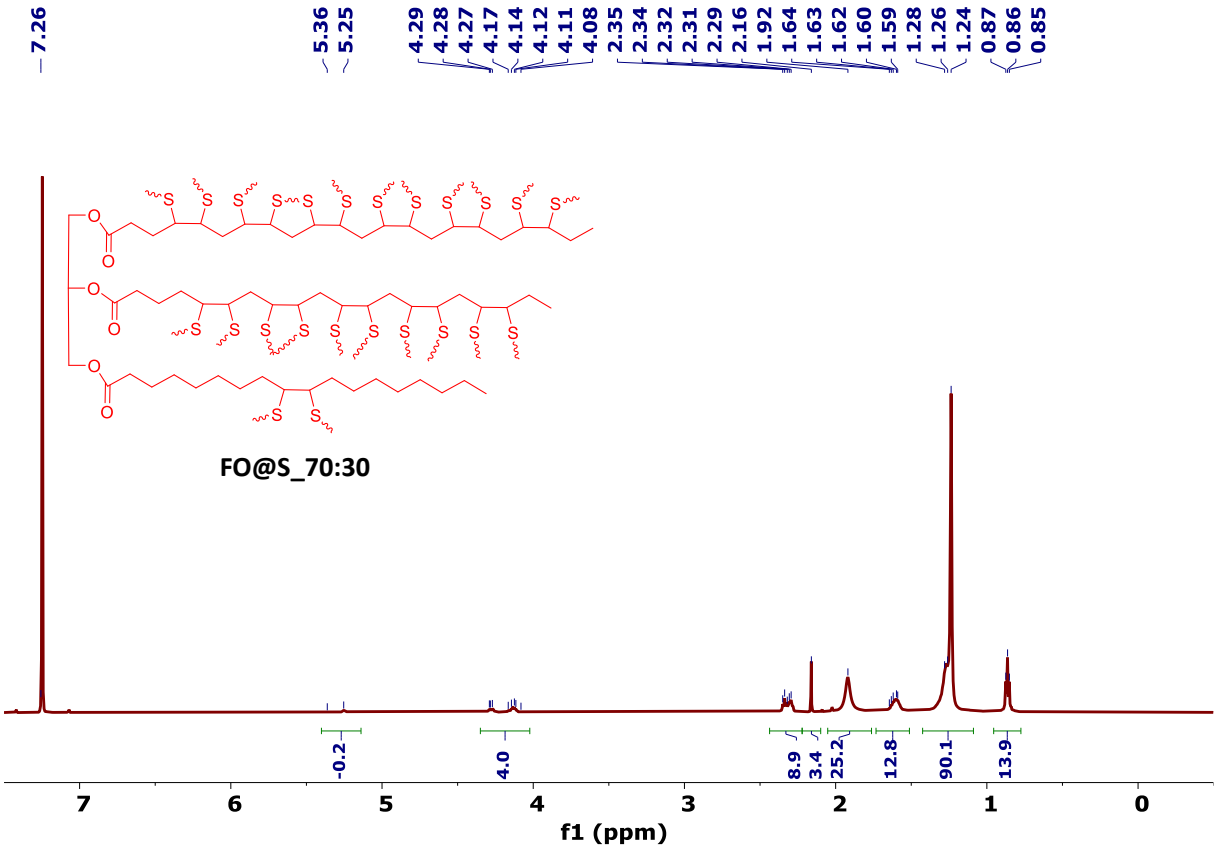

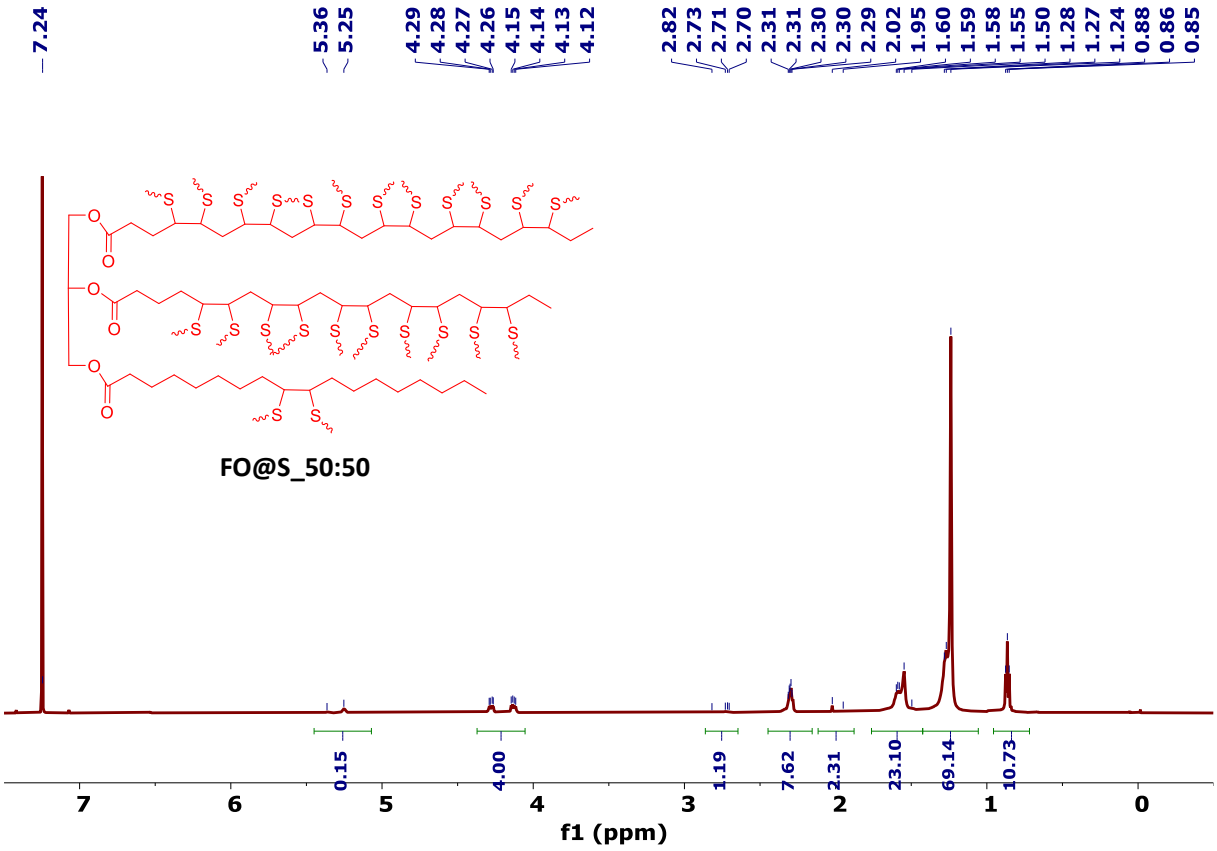
7.24
5.36
5.25
4.29
4.28
4.27
4.26
4.15
4.14
4.13
4.12
2.82
2.73
2.71
2.70
2.31
2.31
2.30
2.30
2.29
2.02
1.95
1.60
1.59
1.58
1.55
1.50
1.28
1.27
1.24
0.88
0.86
0.85
FO@S_50:50
0.15
4.00
1.19
7.62
2.31
23.10
69.14
10.73
7
6
5
4
3
2
1
0
f1 (ppm)

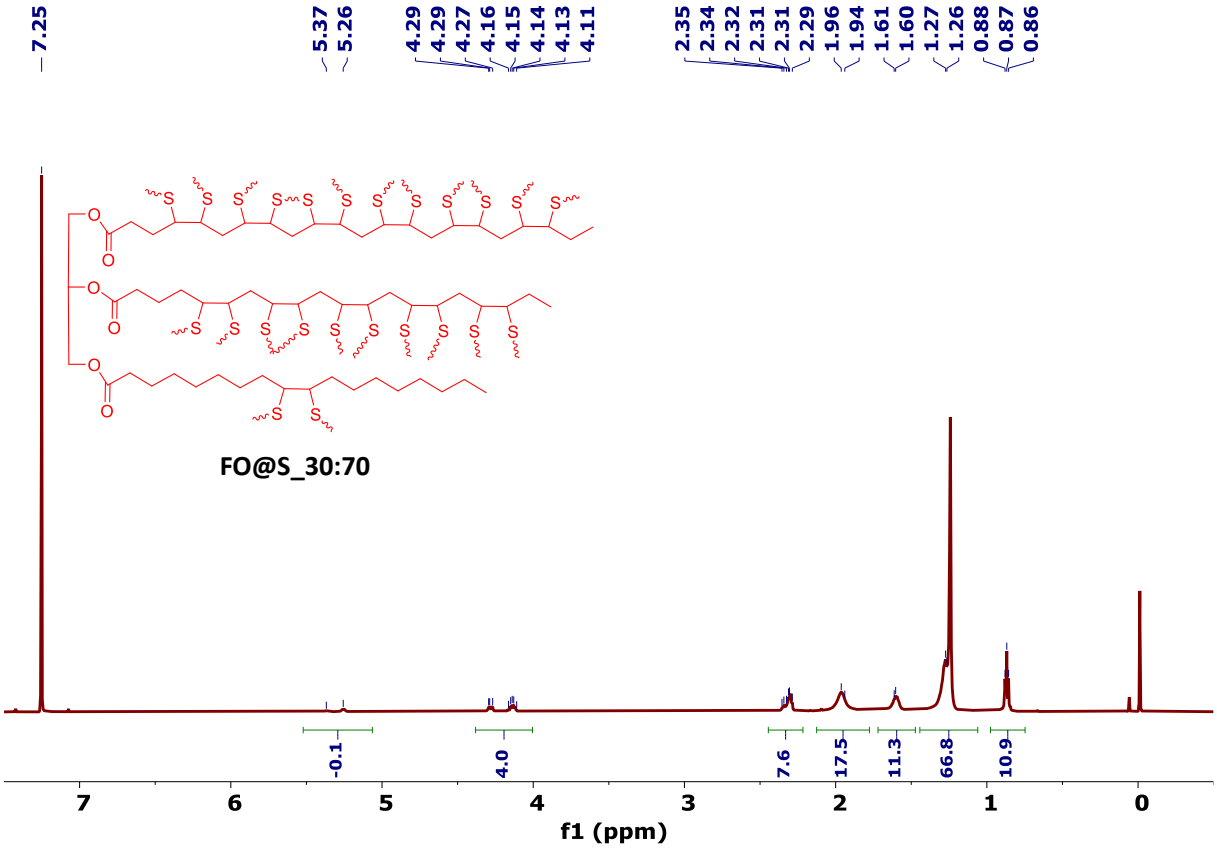
7.25
5.37
5.26
4.29
4.29
4.27
4.16
4.15
4.14
4.13
4.11
2.35
2.34
2.32
2.31
2.31
2.29
1.96
1.94
1.61
1.60
1.27
1.26
0.88
0.87
0.86
FO@S_30:70
-0.1
4.0
7.6
17.5
11.3
66.8
10.9
7
6
5
4
3
2
1
0
f1 (ppm)

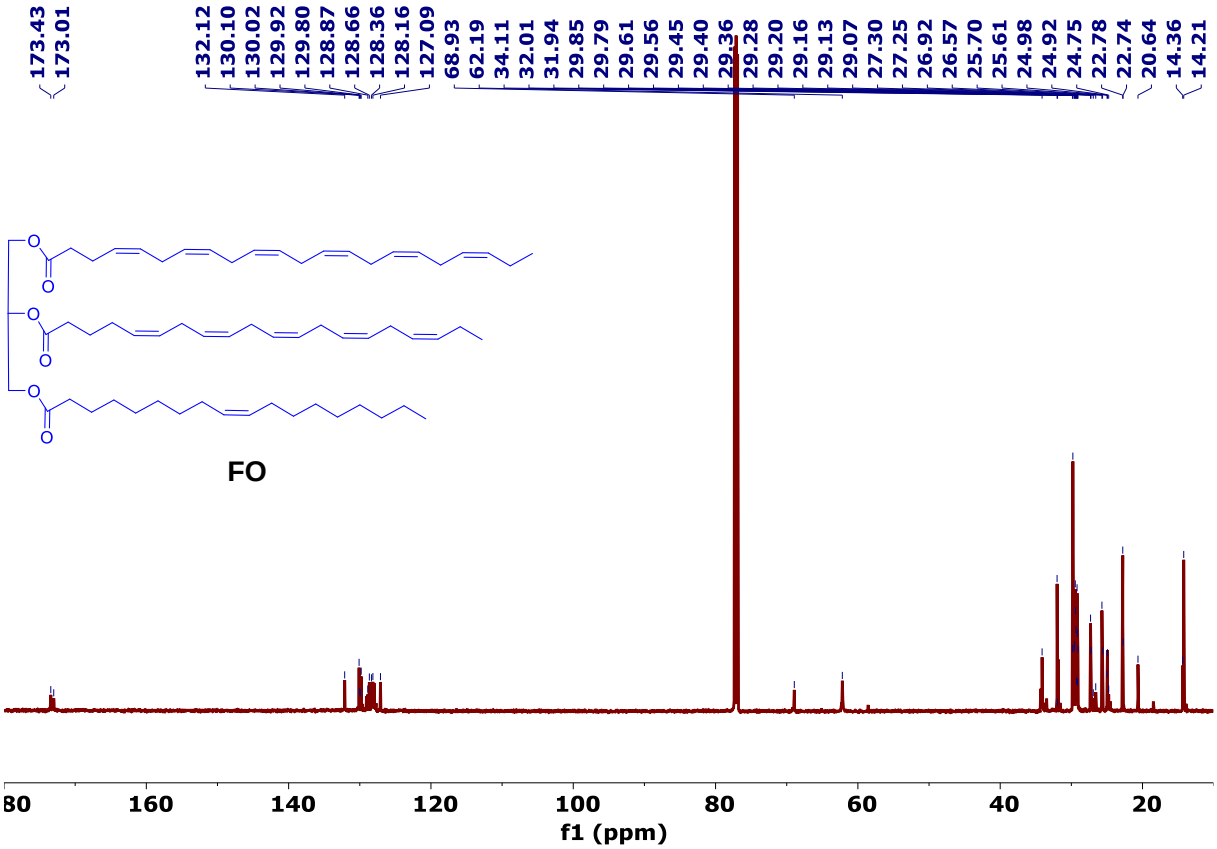
173.43
173.01
132.12
130.10
130.02
129.92
129.80
128.87
128.66
128.36
128.16
127.09
68.93
62.19
34.11
32.01
31.94
29.85
29.79
29.61
29.56
29.45
29.40
29.36
29.28
29.20
29.16
29.13
29.07
27.30
27.25
26.92
26.57
25.70
25.61
24.98
24.92
24.75
22.78
22.74
20.64
14.36
14.21
FO
80
160
140
120
100
80
60
40
20
f1 (ppm)

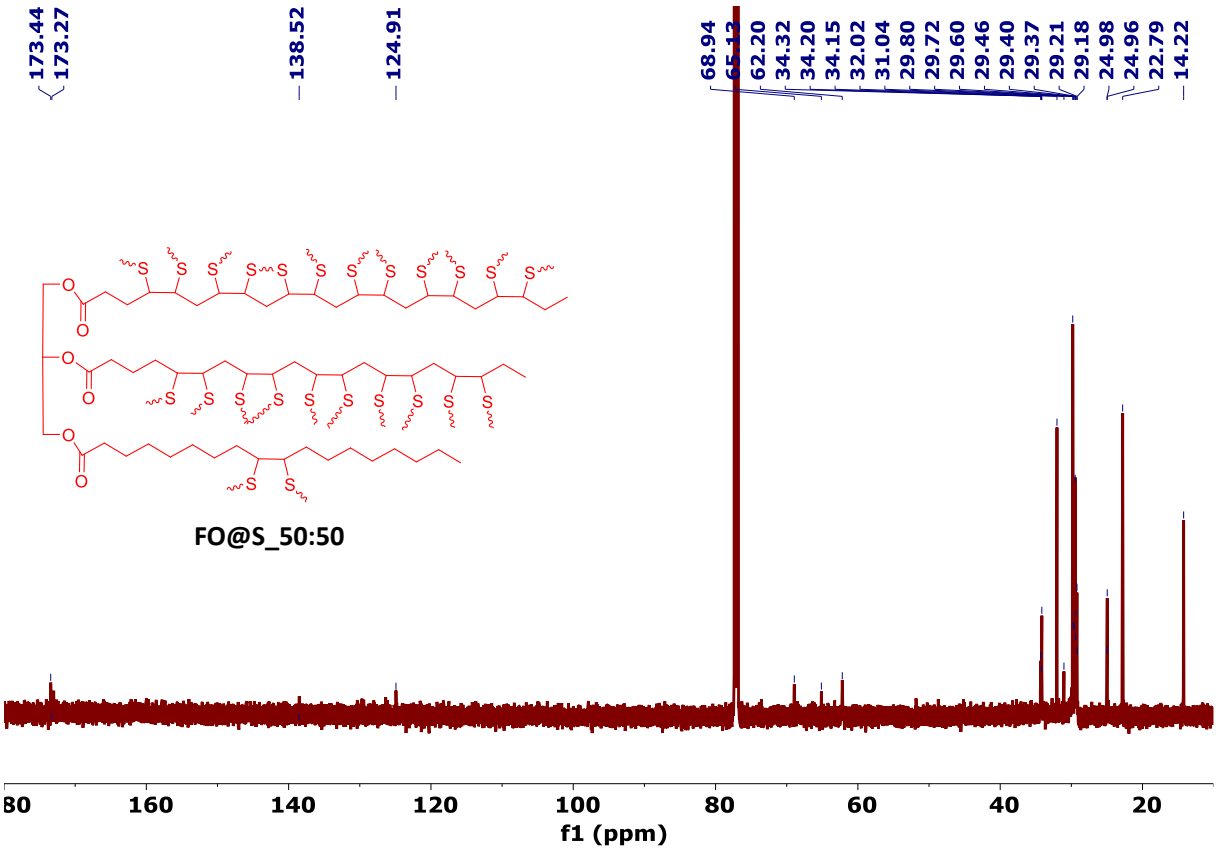
173.44
173.27
138.52
124.91
68.94
65.13
62.20
34.32
34.20
34.15
32.02
31.04
29.80
29.72
29.60
29.46
29.40
29.37
29.21
29.18
24.98
24.96
22.79
14.22
FO@S_50:50
80
160
140
120
100
80
60
40
20
f1 (ppm)

Figure S4. XRD of elemental S8 and **FO@S_X:Y** before removal of unreacted elemental sulfur.

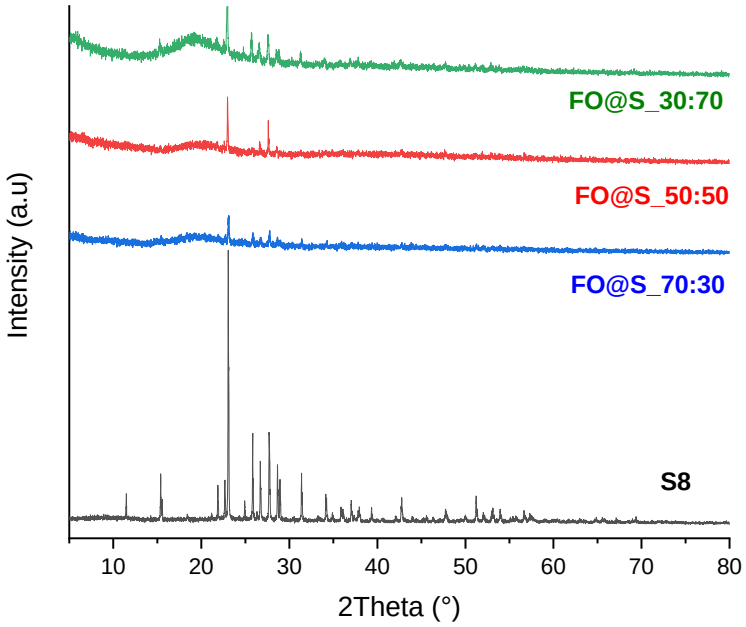

Figure S5. Nitrogen adsorption–desorption isotherms of **FO@S_X:Y**

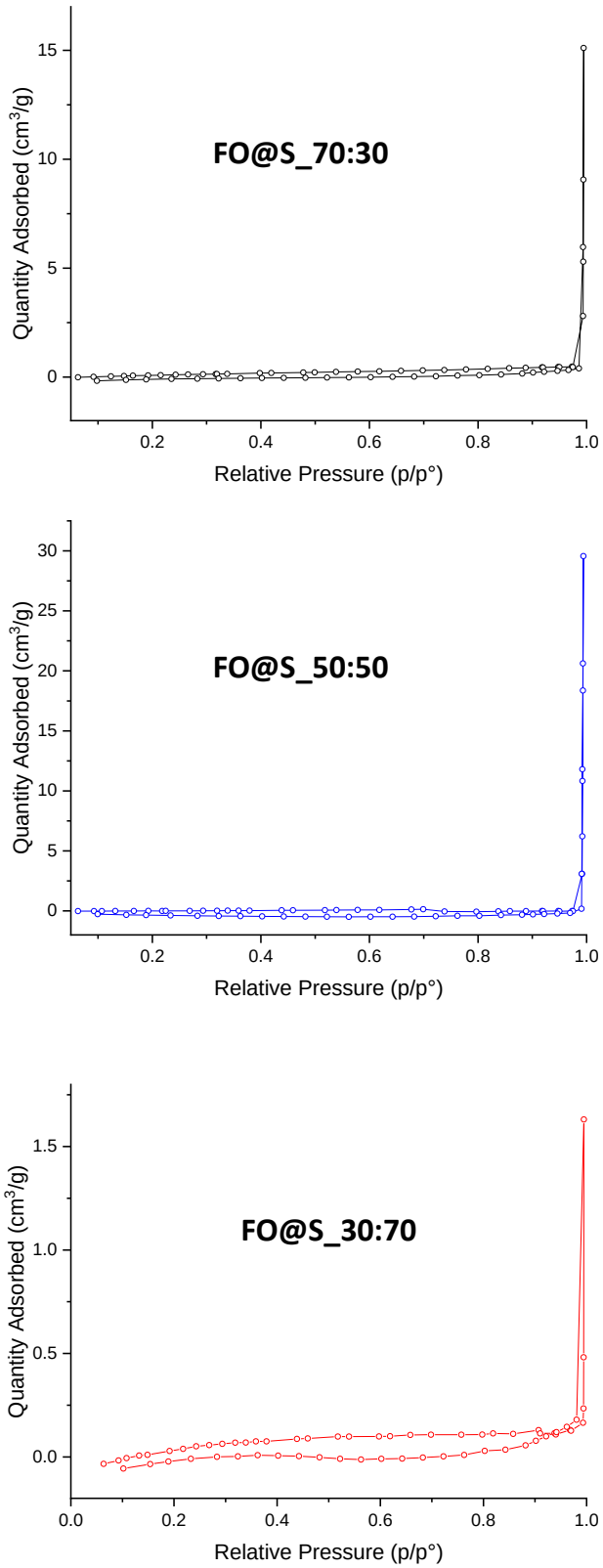

Figure S6. DSC of **FO@S_X:Y**.

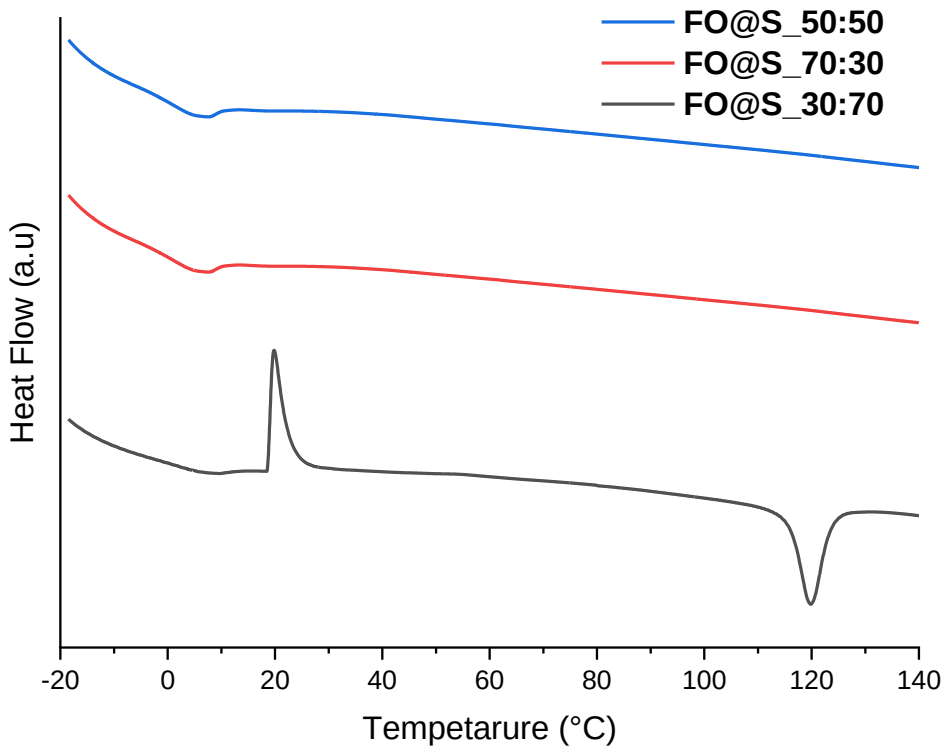

Figure S7. FTIR spectra of **FO@S_50:50-GO** and **FO@S_50:50-MMT.**

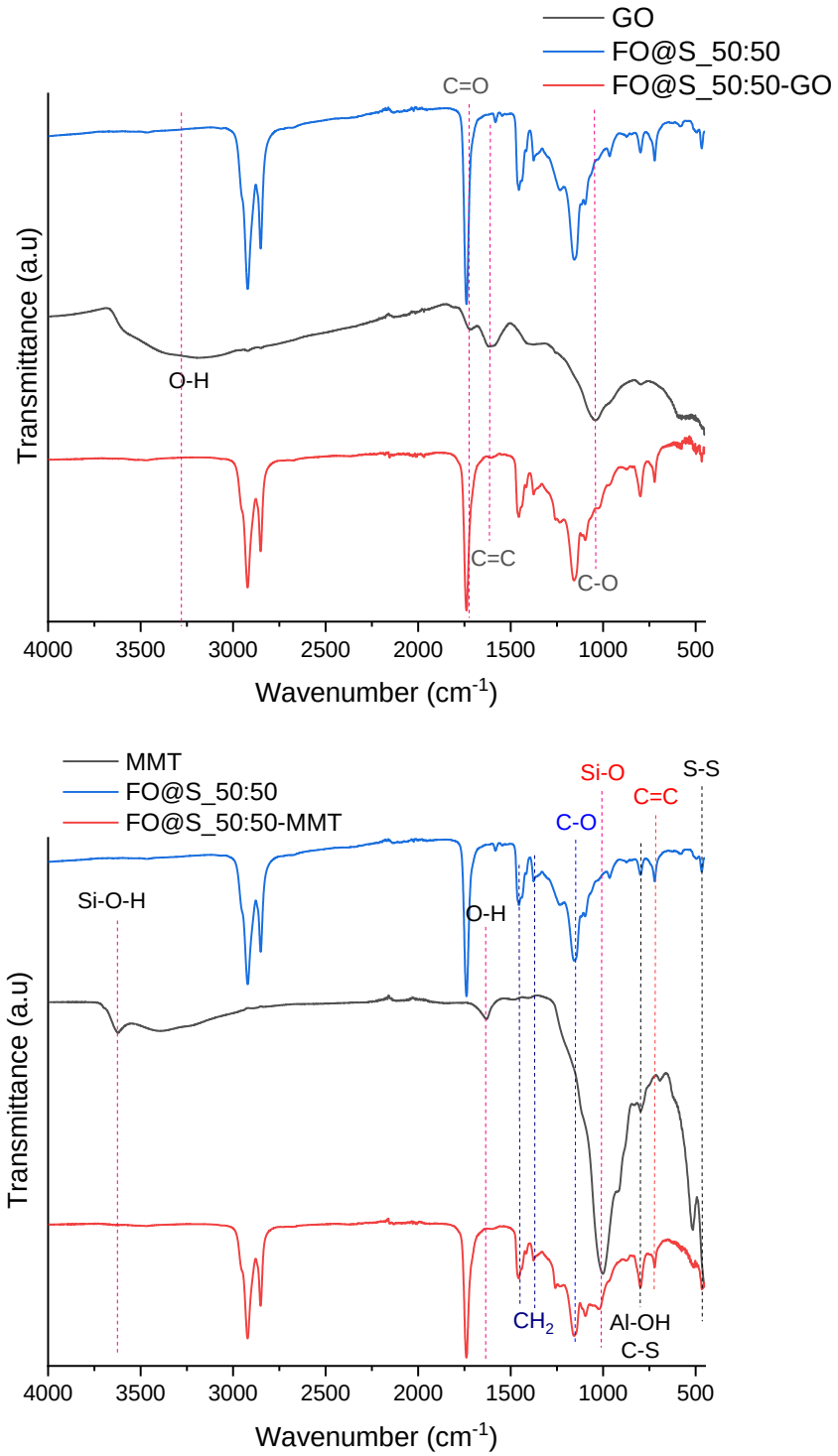

Figure S8. SEM–EDX elemental maps (C, S) of (a) **FO@S_50:50-GO** and (b) **FO@S_50:50-MMT.**

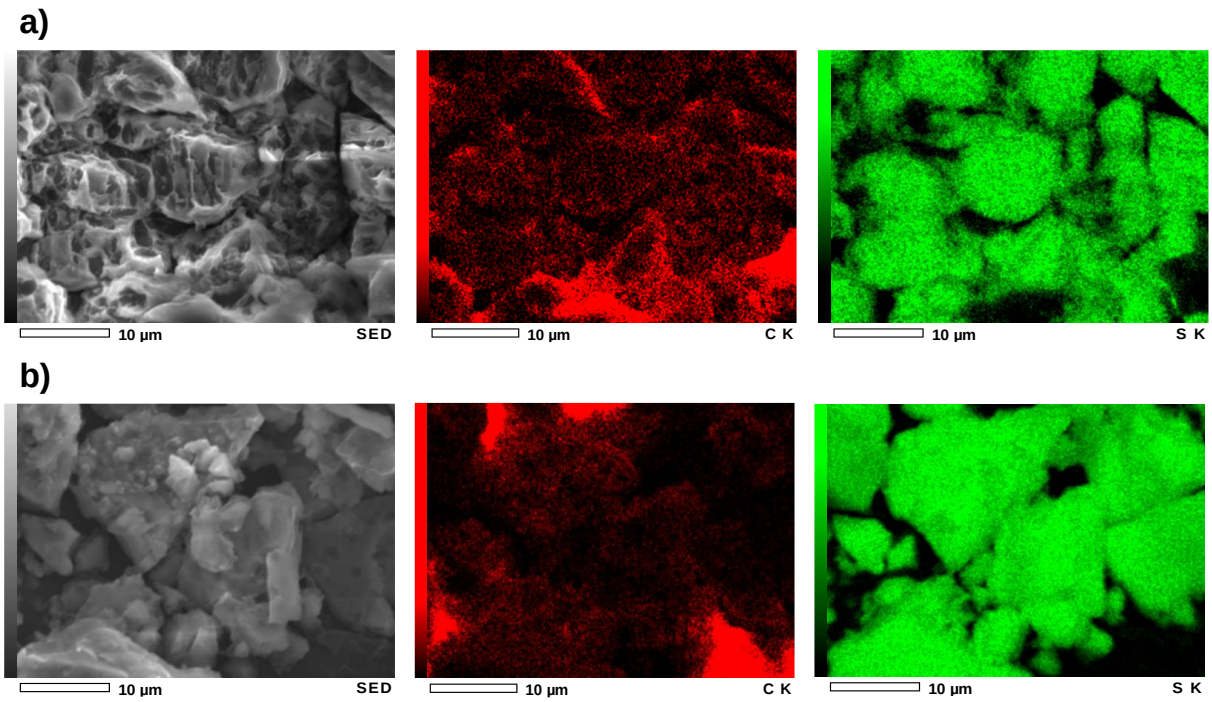

Table S1. Expected and experimental elemental composition (C, H, S, O) and C/H ratio of of **FO@S_X:Y** samples (considering fish oil with the formula $C_{57}H_{104}O_6$ (C = 77.4 wt%, H = 11.8 wt%, O = 10.8 wt%, C/H = 6.56)

Sample	C (exp)	C (found)	H (exp)	H (found)	S (exp)	S (found)	O (exp)	O (found)	C/H (found)
FO@S_70:30	54.18	58.60	8.26	7.93	30.00	24.69	7.56	8.67	7.39
FO@S_50:50	38.70	51.14	5.90	6.98	50.00	35.71	5.40	8.08	7.33
FO@S_30:70	23.20	31.53	3.54	4.13	70.00	58.68	3.24	4.44	7.63

Table S2. Thermogravimetric analysis of FO@S-based composites

Materials	Under air		Under N2	
	T50 (°C)	Residue at 600°C (wt%)	T50 (°C)	Residue at 600°C (wt%)
FO	388	0.0	-	-
S8	264	0.0	-	-
FO@S_70:30	358	0.0	390	11.0
FO@S_30:70	253	0.0	363	11.8
FO@S_50:50	354	0.0	399	10.6
FO@S_50:50-GO	374	0.0	-	-
FO@S_50:50-MMT	382	5.0	-	-

Figure S9. Photographs of **FO@S_50:50** powder in different solvents and acids at room temperature, when 500 mg of material was dispersed in 5 mL of solvent.

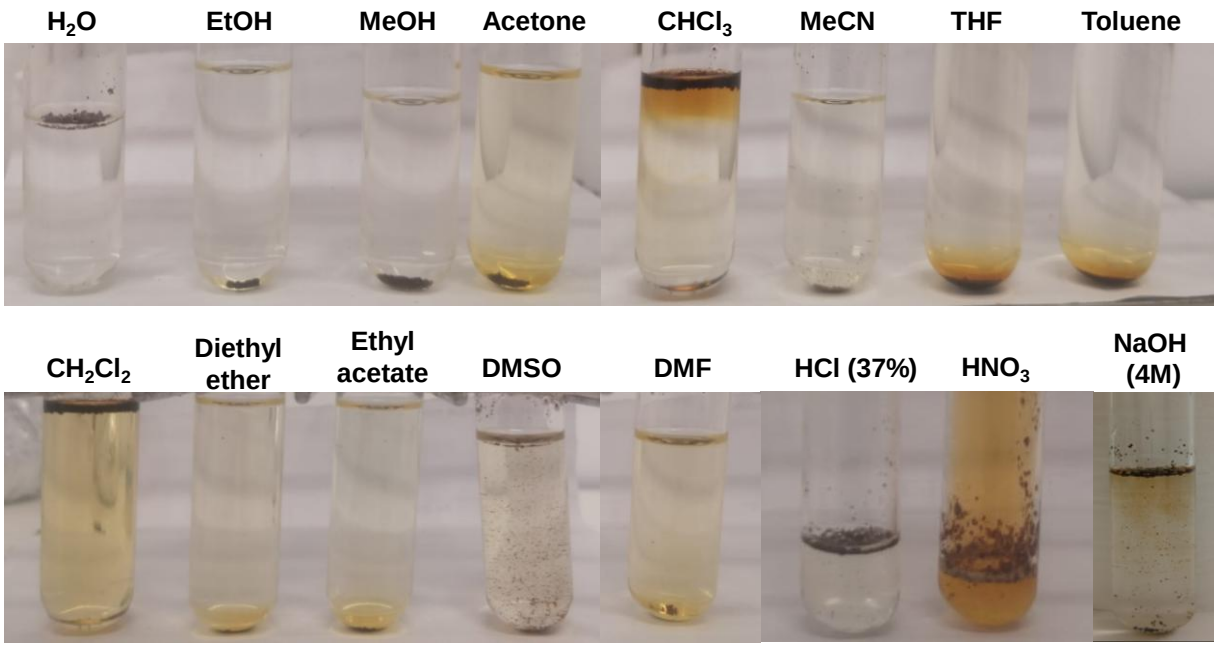

Figure S10. Demonstration of the compressibility and elastic recovery of **FO@S_50:50** foam.

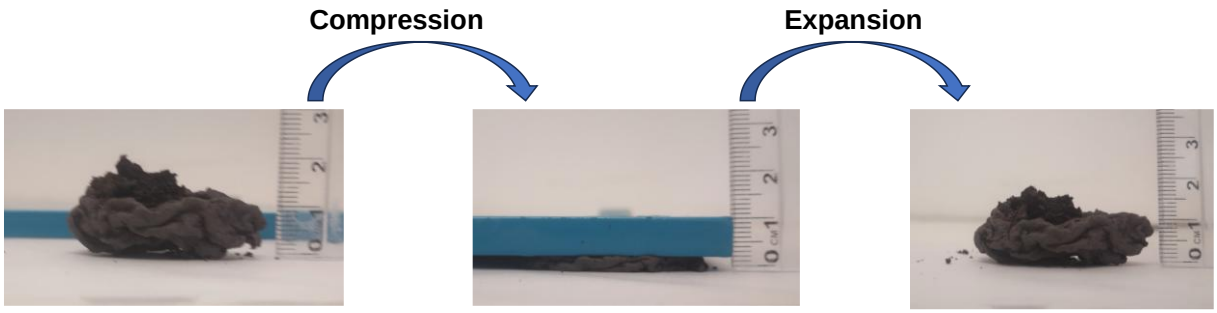

Figure S11. Physical transformation of **FO@S_50:50** from foamed to powdered adsorbent material

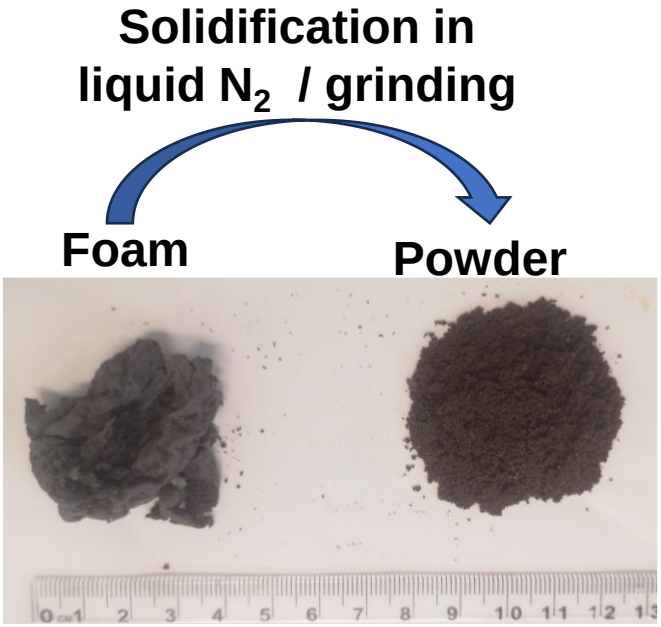

Figure S12. Amount adsorbed of Au(III) and Fe(III) using S_8, **FO@S_X:Y**, **FO@S_50:50-GO** and **FO@S_50:50-MMT.**

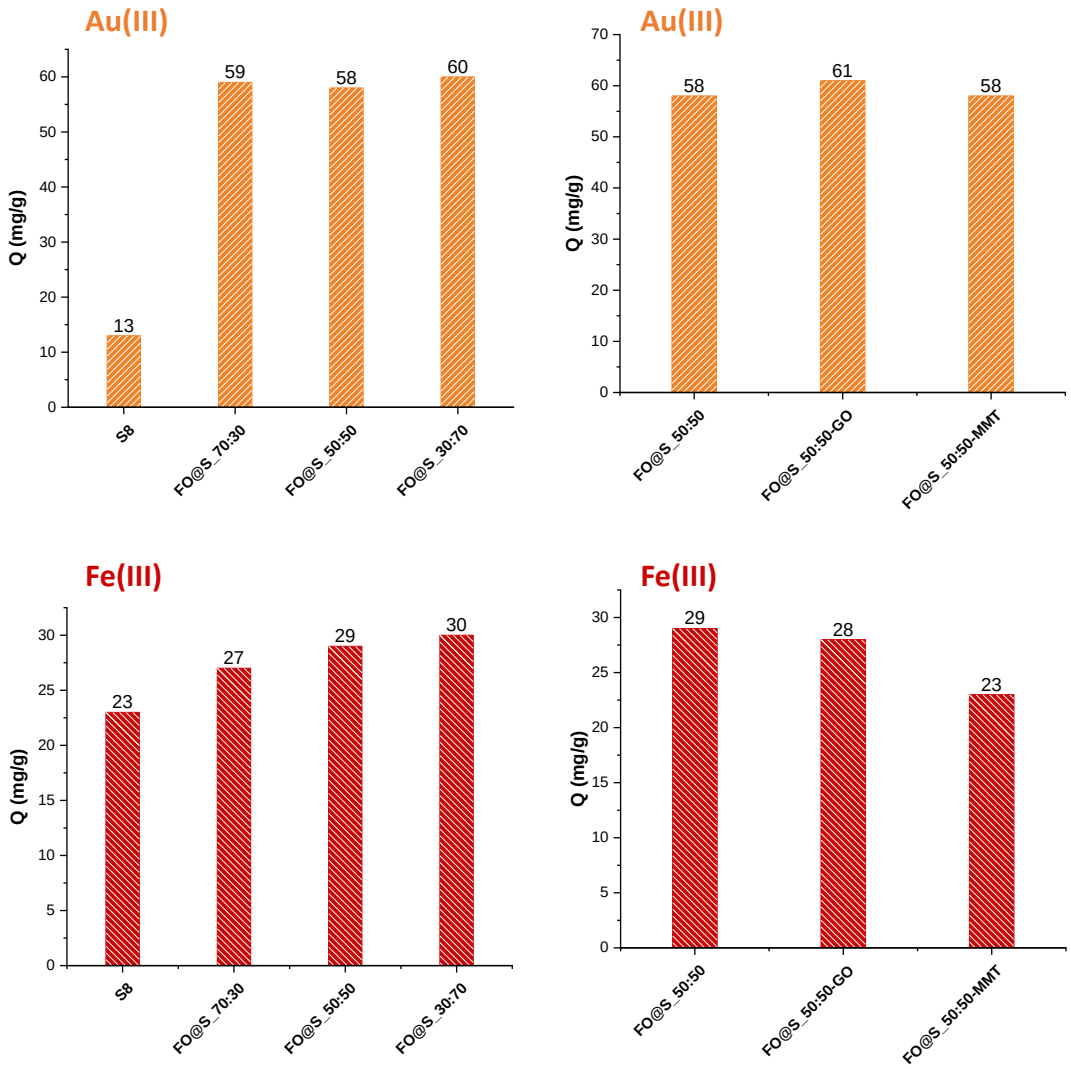

Figure S13. Adsorption isotherm of Fe(III) onto **FO@S_50:50**

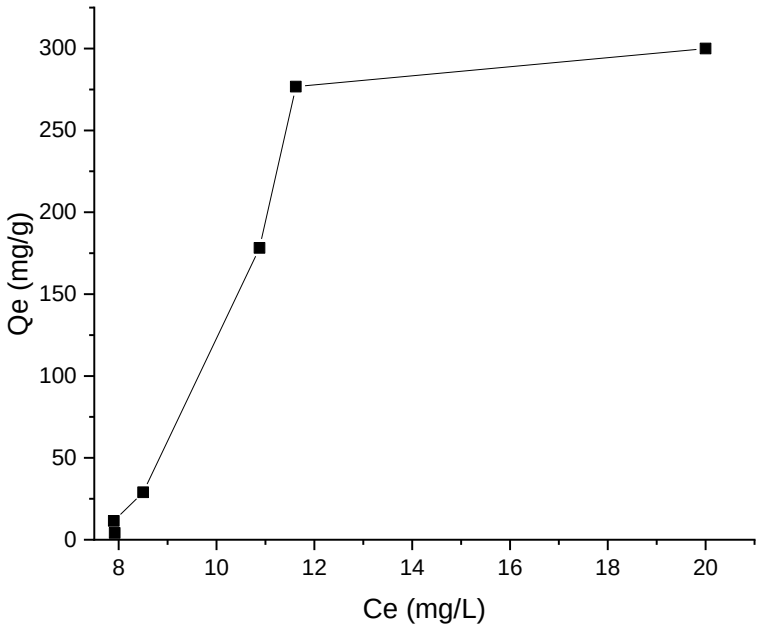

Figure S14. Amount adsorbed of MB using S_8, **FO@S_X:Y**, **FO@S_50:50-GO** and **FO@S_50:50-MMT.**

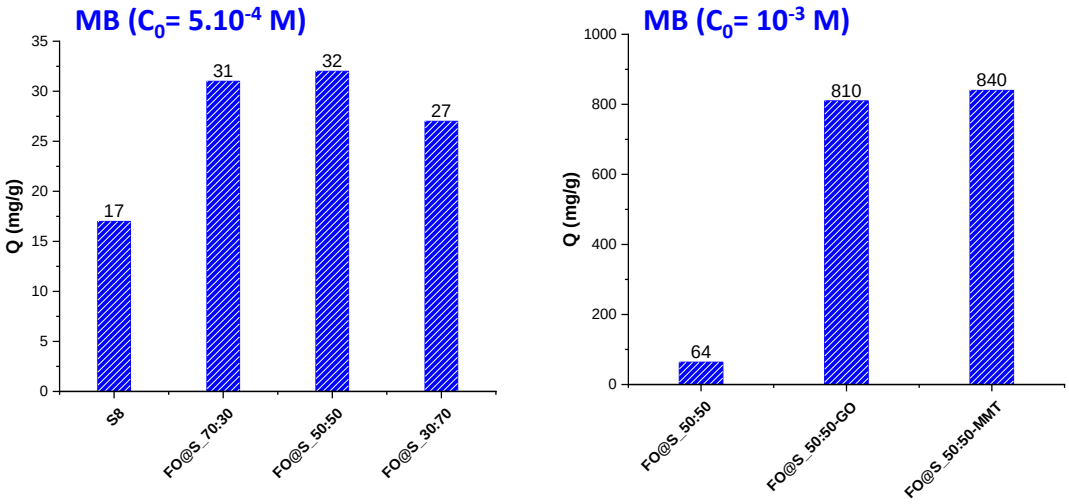

Figure S15. Amount adsorbed of I_2 using **FO@S_X:Y**, **FO@S_50:50-GO** and **FO@S_50:50-MMT.**

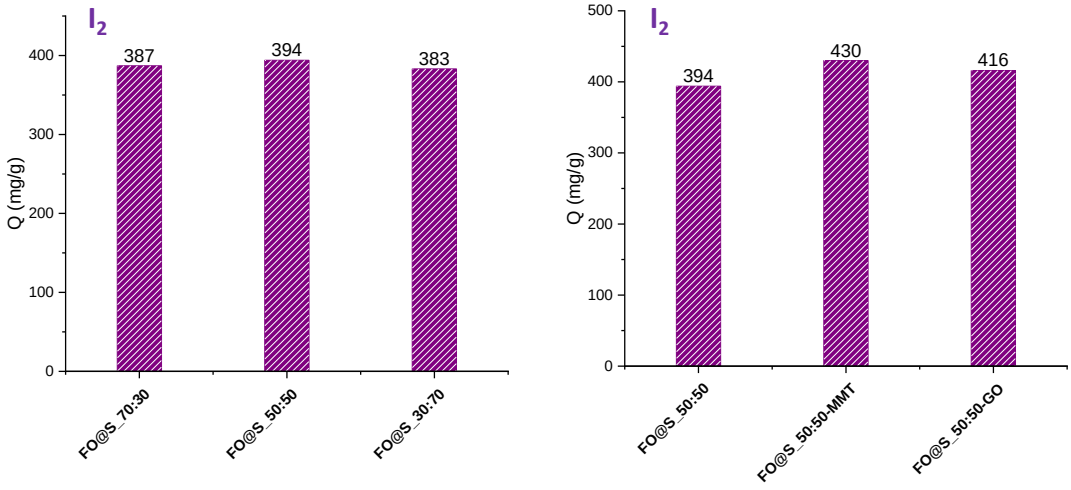

Figure S16. Release of I_2 absorbed by **FO@S_50:50** in ethanol

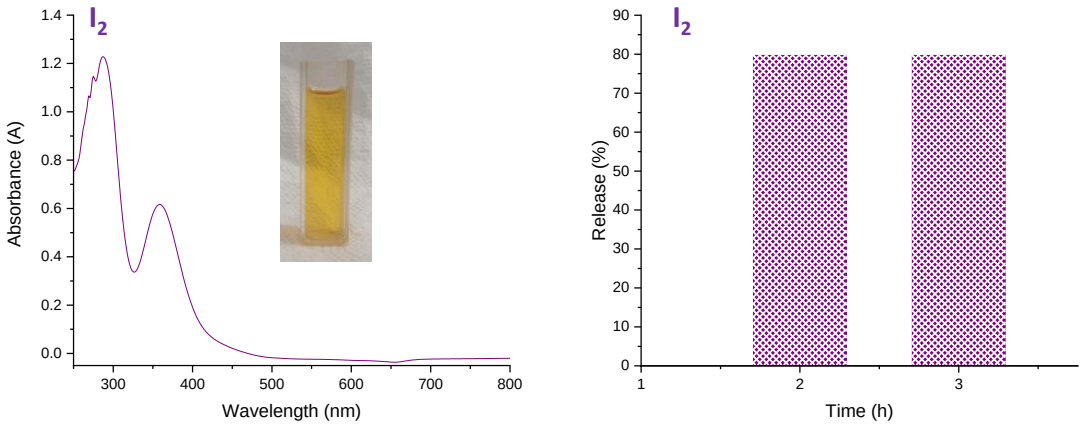

Figure S17. Visual appearance of **FO@S_50:50** powder before and after I_2 adsorption

Before After

Table S3. Comparative adsorption performance of inverse-vulcanized materials and FO@S-based composites toward Au(III), Fe(III), and Methylene blue

Species removed	Monomer	Removal (%) (initial concentration, contact time)	Adsorption Capacity (mg/g)	Ref
Au(III)	Edible blending oil	99.9 (100ppm, 1h)	20.7	[2]
	Diallyl dimethylammonium chloride	94 (1000ppm, 0.5h)	602	[3]
	1,4-butadiyl-3,3′-di-1-vinylimidazole bromide	99 (200ppm, 8h)	636.5	[4]
	FO@S_50:50	94 (178ppm, 24h)	58	This work
	FO@S_50:50-GO	99 (178ppm, 24h)	61	
	FO@S_50:50-MMT	96 (178ppm, 24h)	58	
Fe(III)	Canola oil	95 (50 ppm, 24h)	0.8	[5]
	Dipentene, garlic oil, diallyl disulfide, and myrcene	83 (100ppm, 24h)	-	[6]
	FO@S_50:50	95 (17ppm, 24h)	29	This work
	FO@S_50:50-GO	94 (17ppm, 24h)	28	
	FO@S_50:50-MMT	79 (17ppm,24h)	23	
Methylene blue	1,3-diisopropenylbenzene	96 (8ppm, 3h)	7.7	[7]
	FO@S_50:50	99 (160ppm, 24h)	32	This work
		10 (320ppm, 24h)	64	
	FO@S_50:50-GO	96 (320ppm, 24h)	810	
	FO@S_50:50-MMT	99 (320ppm, 24h)	840	

References

1. W. S. Hummers Jr and R. E. Offeman, *J. Am. Chem. Soc.*, 1958, **80**, 1339-1339.
2. Z. Ren, X. Jiang, L. Liu, C. Yin, S. Wang and X. Yang, *J. Mol. Liq.*, 2021, **328**, 115437.
3. M. L. Eder, C. B. Call and C. L. Jenkins, *ACS Appl. Polym. Mater.*, 2022, **4**, 1110-1116.
4. X. Zhou, Y. Cui, X. Xun, J. Jia, X.-C. Wang and Z.-J. Quan, *Sep. Purif. Technol.*, 2025, **365**, 132679.
5. N. A. Lundquist, M. J. Worthington, N. Adamson, C. T. Gibson, M. R. Johnston, A. V. Ellis and J. M. Chalker, *RSC Adv.*, 2018, **8**, 1232-1236.
6. S. Silvano, I. Tritto, S. Losio and L. Boggioni, *Polym. Chem.*, 2022, **13**, 2782-2790.
7. M. Wu, Y. Liu, L. Wu, T. Hasell and F. Luan, *RSC Adv.*, 2025, **15**, 13225-13234.